Intermolecular Electron Transfer on the Surface of MgO Nanoparticles

O. Diwald and E. Knözinger*

Institut für Physikalische und Theoretische Chemie, Technische Universität Wien, c/o Veterinärplatz 1/GA, A-1210, Wien, Austria

Received: March 20, 2001; In Final Form: January 24, 2002

A systematic study of electron-transfer reactions on the surface of MgO nanoparticles, exposed to H_2/O_2 atmosphere in the dark, was performed. The evolving products are two different types of surface complexes consisting each of a paramagnetic superoxide anion (O_2^-) on a Mg^{2+} cation and an adjacent infrared active hydroxyl group (OH). Via the electronic (H-bond-like) influence of O_2^- on the OH group (red shift of the respective IR signal) the process of O_2^- evolution can be monitored IR spectroscopically on a time scale of minutes. Additional structural information on the complexes is obtained via the magnetic influence of the OH proton on O_2^- (superhyperfine splitting of the respective EPR signals). On the bases of these data as well as on a kinetic evaluation of the time-dependent IR and EPR signals, a description of two local surface structures involved in a complicated reaction scheme was obtained: two hydride groups as intermediate products are constituents of a low coordinated anion vacancy or of a (110) microplane, respectively. A fraction of the products ($O_2^-\cdots HO$) is located on ion pairs adjacent to or in these structure elements. Because of an intermediately produced mobile H radical, further product evolves on similar ion pairs (same coordination), but remote from the local surface structures where H_2 may be split.

Introduction

Magnesium oxide (MgO) is a homomorphous compound with rocksalt structure. Its ionic constituents comprise a relatively small number of electrons and dispose of stable oxidation states. Owing to these properties MgO surfaces are likely to exhibit a limited number of reasonably well-defined surface defect structures such as low coordinated ions[1−3] and/or vacancies.[4−6] As a consequence, in the recent past both theoreticians and experimentalists have developed an overwhelming interest for MgO which has become one of the preferred targets of surface structural and catalytic research.[7−9]

Molecular hydrogen is an efficient IR probe for the characterization of low coordinated cation−anion pairs.[10−12] It is known that two types of H_2 chemisorption complexes, each incorporating a $Mg^{2+}-H^-/O^{2-}-H^+$ pair, can be observed in the dark on highly dispersed MgO samples. One stems from an—at room temperature—irreversible splitting process (eq 1a) and is related to two IR bands ν(OH) at 3712 and ν(MgH) at 1130 cm^{-1} (Figure 1a). This chemisorption complex, which is designated in the following text as complex **I**, is already saturated at H_2 pressures ≤ 0.1 mbar.

$$\text{complex } \mathbf{I}: \quad (O^{2-}_{LC}-Mg^{2+}_{LC})_{\mathbf{I}} + H_2 \rightarrow O^{2-}(H^+)_{\mathbf{I}}-Mg^{2+}(H^-)_{\mathbf{I}} \tag{1a}$$

In addition, a second and—at room temperature—reversible splitting process gives rise to the appearance of bands ν(OH) at 3462 and ν(MgH) at 1325 cm^{-1} (Figure 1a) that manifest the presence of complex **II**.

$$\text{complex } \mathbf{II}: \quad (O^{2-}_{LC}-Mg^{2+}_{LC})_{\mathbf{II}} + H_2 \rightarrow O^{2-}(H^+)_{\mathbf{II}}-Mg^{2+}(H^-)_{\mathbf{II}} \tag{1b}$$

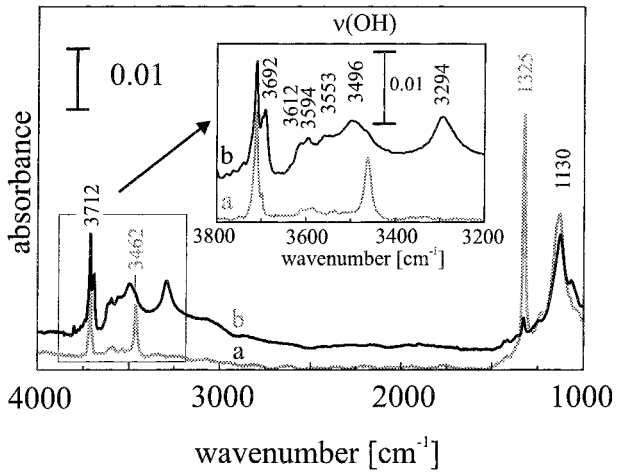

Figure 1. IR spectrum of MgO exposed to (a) 100 mbar H_2 (b) 100 mbar of a H_2/O_2 mixture (ratio 95:5). The spectra were recorded at 298 K 10 min after gas admission.

It is—different from complex **I**—not saturation limited within the H_2 pressure range 1 mbar $\leq p \leq$ 100 mbar. The respective OH stretching frequency (3462 cm^{-1}) clearly indicates H-bond interaction. On the other hand, the bandwidth is unusually small for H bonded OH groups, reflecting the rigidity of the MgO surface framework in which the proton donor and the proton acceptor are incorporated.[11]

Both types of resulting surface hydrides (H^-) are reactive toward molecular oxygen. So far only the reaction between the irreversible hydride of complex **I** and molecular oxygen has been studied in the course of so-called *preadsorption* experiments:

$$O^{2-}(H^+)_{\mathbf{I}}-Mg^{2+}(H^-)_{\mathbf{I}} + O_2 \rightarrow O^{2-}(H^+)_{\mathbf{I}}-Mg^{2+}(O_2^-[\mathbf{A}]) + H^\bullet \tag{2a}$$

* To whom correspondence should be addressed. E-mail:erich.knoezinger@tuwien.ac.at. Fax: 0043-1-25077-3890.

10.1021/jp011049+ CCC: $22.00
Published on Web 03/12/2002

TABLE 1: Relevant Parameters of the EPR Spectra of the Superoxide Anion Species A and B (77 K) and of the IR Spectra of OH Groups (298 K) Interacting with A and B on MgO Surfaces

O_2^- species						OH group
			A			
g_{xx}	g_{yy}	g_{zz}	a_{xx} [G]	a_{yy} [G]	a_{zz} [G]	$\nu_{(OH)}$ [cm^{-1}]
2.0019	2.0085	2.0902	5.10	2.97	1.40	3702
			B			
2.0017	2.0086	2.0769	3.76	2.06	1.10	3692

This type of procedure comprises two separate steps, namely, the H_2 chemisorption according to complex **I** (eq 1a) which remains after evacuation and then the O_2 admission.[13−16] The respective OH group now absorbs at 3702 instead of 3712 cm^{-1} (see above), indicating the interaction with a weak proton acceptor ([11] Table 1), i.e., O_2^-. The reaction according to eq 2a depends on the ionization energy of the respective anion, which should not exceed the value of electron affinity of molecular oxygen. As O_2^- is paramagnetic its occurrence may be evidenced by EPR spectroscopy.[17,18] The orthorhombic symmetry of the spin center is revealed by three principal values of the **g** matrix. Among them only the low-field component g_{zz} sensitively depends on the coordination state of the complexing cation.[17,19] Whether the Mg^{2+} cations on the left and the right side of eq 2a are the same or not, is still an open question.[16]

The formation of O_2^- ions has previously been subject of intense EPR and IR studies aiming at the oxidation of surface color centers on MgO nanoparticles with molecular oxygen.[11,16,20] In general two dominating types of O_2^-, namely, **A** and **B** (see Table 1), have been isolated. Furthermore, a distinct dipolar magnetic interaction between the spin center and a proton of a nearby hydroxyl group was observed at 77 K.[11,16,21] It gives rise to superhyperfine splitting (shf) of the resonance components attributed to the O_2^- radical.[21] Of course, there is also Coulombic attraction between these surface groups which enables one to detect the presence of O_2^- species by IR spectroscopy.[20] Two OH bands with positions slightly below the absorption of free and isolated OH groups indicate the close vicinity of O_2^- species as weak proton acceptors. One of them is the above-mentioned OH band at 3702 cm^{-1} (Table 1).

The aim of the present study is to go into more detail in the study of the redox reactions occurring on the surfaces of MgO nanoparticles exposed to H_2/O_2 mixtures in the dark. Particular attention will be paid to the reaction between the reversibly formed hydride (eq 1b) and molecular oxygen. Another question refers to the so far unclear fate of the H$^\bullet$ radical in eq 2a.[22,23]

Experimental Section

All experiments were carried out with the same type of MgO produced by chemical vapor deposition in a flow reactor system.[24] High purity Mg pieces as educt were supplied by Johnson Matthey GmbH. The specific surface area of the resulting MgO material determined by BET (LN_2) measurements is around 400 m^2/g. To guarantee a totally dehydroxylated surface, the sample was gradually annealed at 1173 K under dynamic vacuum ($<10^{-5}$ mbar) before each experiment. This leads to a reduction of the specific surface area to 320 m^2/g. The rate of temperature increase for the annealing steps was 10 K/min. All samples were treated at 870 K with oxygen in order to burn organic contaminants originating from the oil of the vacuum pumps used in the flow system.

The gases H_2 (99.999%) and $^{16}O_2$ (99.998%) for adsorption studies were provided by Messer Griesheim. The IR and EPR sample cells are connected to an appropriate high vacuum pumping rack. It allows thermal activation of the sample at less than 10^{-5} mbar and 1173 K as well as adsorption/desorption experiments with diverse gases. For the IR experiments small quantities of MgO powder (20−30 mg) were pressed into self-supporting pellets. The pressure applied was less than 10 bar and did not initiate any change of the specific surface area. For the EPR experiments similar amounts of the MgO sample batch, also used for IR spectroscopy, was filled in EPR tubes.

The IR spectra were recorded using a Fourier transform-IR spectrometer model IFS 113v (Bruker Optik GmbH). The resolution was 3 cm^{-1}. Three hundred interferogram scans were averaged in order to guarantee a reasonable signal-to-noise ratio. The reference for the absorbance spectra is a MgO sample previously subjected to thermal activation and then cooled to room temperature. The EPR spectra were obtained on a Bruker EMX 10/12 spectrometer system in the X band. The spectra presenting paramagnetic oxygen species required a reduction of the temperature to 77 K in order to avoid line broadening. In this case 10 coadded spectra sufficed to obtain a satisfactory signal-to-noise ratio. The DPPH signal as well as the lines originating from traces of Mn^{2+} in the sample were applied for g value calibration.

A considerable part of the kinetic studies is based on the time dependence of the intensity of overlapping OH stretching bands in the interval between 3710 and 3690 cm^{-1} (Figures 2 and 8). They have to be fitted by 3 Gaussian/Lorentzian curves according to a least squares procedure. The band parameters (position, width at half-height and shape in terms of Gaussian/Lorentzian contributions) of two of them—3702 and 3692 cm^{-1}—are known from independent experiments.[11,20] The third one (3710 cm^{-1}) is a comparatively weak feature. Thus the integrated absorbance values of the two major constituents of the complex band around 3700 cm^{-1} is in principle readily available for the kinetic studies.

Results

The IR spectrum obtained after coadsorption of H_2 (1 mbar $\leq$ p(H_2) $\leq$ 100 mbar) and 5 mbar O_2 on CVD MgO (Figure 1b) exhibits dramatic differences from that related to the chemisorption of pure H_2 at the same partial pressure (Figure 1a). The intensity of the band attributed to the irreversible hydride group (1130 cm^{-1}) is reduced significantly, whereas the MgH band originating from the reversible H_2 chemisorption (1325 cm^{-1}) has completely vanished. The same is true for the OH band of complex **II** (eq 1b) at 3462 cm^{-1} which merges into a slightly structured continuous absorption in the range between 3650 and 3300 cm^{-1}. The whole absorption pattern after H_2/O_2 coadsorption does not change at all when $^{18}O_2$ instead of $^{16}O_2$ is added.[25] The absence of any experimental $^{16}O/^{18}O$ isotope effect evidences that the molecular oxygen does not provide the oxygen atom for the OH groups exhibiting the continuous absorption.[25] This feature must be related to a so far unknown H bond network. It grows monotonically with H_2 pressure.

Specific spectral changes related to the electron-transfer reaction become observable in the difference mode (Figure 2), where the spectrum obtained in the presence of pure hydrogen is subtracted from that related to coadsorption of H_2 and O_2. Two relatively sharp, overlapping positive bands at 3702 and 3692 cm^{-1} appear. They have previously been observed in the course of the oxidation of surface color centers on MgO with molecular oxygen.[11,16,20] Their positions—slightly red-shifted with respect to free and isolated OH at 3712 cm^{-1}—were explained by an H bond like interaction with superoxide

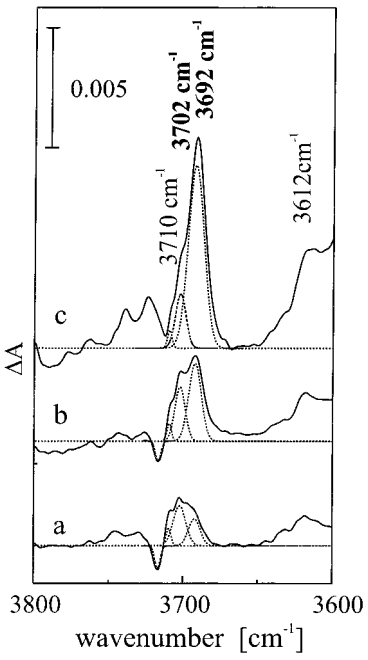

Figure 2. IR difference spectra recorded in the OH stretching region of MgO after surface reaction with $H_2/O_2/N_2$ mixtures at 298 K (time scale: 0−4 min after gas admission). Gas composition: (a) $p(H_2):p(O_2):p(N_2)$ = 1:5:94 mbar, (b) $p(H_2):p(O_2):p(N_2)$ = 5:5:90 mbar, and (c) $p(H_2):p(O_2):p(N_2)$ = 95:5:0 mbar. (N_2 was added in order to guarantee constant total pressure conditions). Each curve was obtained by subtracting the absorbance spectrum related to chemisorption of pure H_2 from that related to chemisorption of H_2 plus O_2 (same H_2 pressure in both experiments).

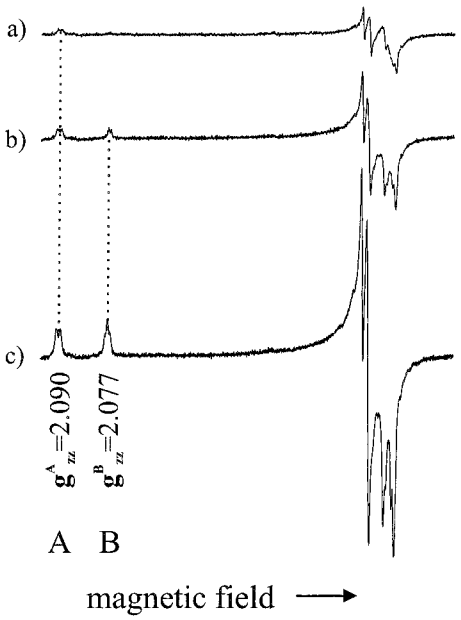

Figure 3. EPR spectra of superoxide anions recorded at 77 K. The O_2^- species were produced by the admission of $H_2/O_2/N_2$ mixtures (same compositions as in Figure 2a−c, respectively) to the MgO sample for 40 min at 298 K.

anions O_2^-. In fact, EPR studies paralleling the above-described IR experiments in the dark unambiguously evidence the presence of the O_2^- species **A** and **B** as a result of the coadsorption of H_2 and O_2 (Figure 3).[26] Both **A** and **B** exhibit (at 77 K) the distinct shf splitting known from the result of color center bleaching by molecular oxygen on MgO surfaces (refs 11 and 16, see Introduction) Thus, we may complement eq 2a by a similar reaction scheme that is related to the complex **II**:

$$O^{2-}(H^+)_{II}-Mg^{2+}(H^-)_{II} + O_2 \rightarrow O^{2-}(H^+)-Mg^{2+}(O_2^-[\mathbf{B}]) + H^\bullet \quad (2b)$$

Different from eq 2a the OH group on the right side of eq 2b may, but has not necessarily to be the one which originates from the respective H_2 splitting process (complex **II**). This will be discussed later on (eq 3).

The synopsis of the IR and EPR data presented here suffers from a fundamental difference in the effect of thermal motion of the O_2^- species.[27,28] At room-temperature intermolecular vibrations of O_2^- are thermally strongly excited and create a relatively unspecific structure of the EPR signal components[29] which do not allow a reliable discrimination of different O_2^- species. Therefore, the EPR spectra were recorded at 77 K. On the other hand, the IR detection of O_2^- is based on the electronic, H-bond like interaction between the OH dipole and O_2^-. This interaction mainly depends on the distance between the centers of gravity of the related charge densities and is essentially not affected by the intermolecular vibrations of O_2^-. Thus the IR spectra provide relevant information also at room temperature (cryogenic equipment which would allow to carry out the IR studies at 77 K has not been available in our lab for the present project.)

The interpretation and the evaluation of the IR pattern around and above 3692 cm^{-1} has to be carried out with extreme care. The features observed there are the result of spectral subtraction and of subsequent band fitting. The respective intensity values amount to a few thousands of an absorbance unit. Therefore, both statistical and systematic errors are likely to play a nonnegligible role. To avoid misinterpretations, exclusively those features were taken into account which are stable in frequency and exhibit systematic trends in band intensity on varying well-defined and reliably monitored experimental conditions such as the partial pressure of H_2 (Figure 2) and O_2 (Figure 8). Only the positive difference bands at 3702 and 3692 cm^{-1} are in agreement with these requirements. The small positive feature at 3710 cm^{-1} remains essentially unchanged, whereas the negative one at 3718 cm^{-1} is not frequency stable (Figure 8). At this point it has to be mentioned that under special experimental conditions, different from those applied here, isolated surface OH groups embedded in very specific MgO surface environments are observed at 3718, 3745, and 3762 cm^{-1}.[30] However, according to the control procedure applied to the data of Figures 2 and 8, the features observed there in the interval between 3718 and 3762 cm^{-1} are not significant and do not interfere in the evaluation of the difference bands at 3702 and 3692 cm^{-1}.

Both IR and EPR spectra sensitively depend on the H_2 partial pressure during the coadsorption experiment (Figures 2 and 3, respectively) and on time (Figures 4−6). Different from the band at 3702 cm^{-1}, the one at 3692 cm^{-1} grows with $p(H_2)$ in the range from 1 to 100 mbar (Figure 2). On the other hand, the signal components of both superoxide anion species O_2^-[**A**] and O_2^-[**B**] (Figure 3b,c) monotonically gain intensity at the same rate on raising the H_2 partial pressure from 5 to 100 mbar. At 1 mbar only the species O_2^-[**A**] is present (Figure 3a).

The IR bands at 1325 cm^{-1} (Figure 4b) and at 3692 cm^{-1} (Figure 5a−c), as well as the resonance component g_{xx} of the O_2^- species (Figure 6a−c), which is the most significant EPR feature and represents the total amount of superoxide anion species present, are of particular interest. At 298 K their in-

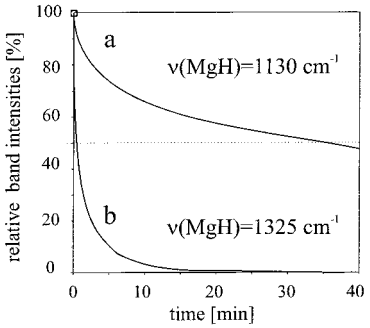

Figure 4. Time dependence of the depletion of the two hydride groups (originating from H_2 chemisorption on MgO, see Figure 1a) by O_2 at 298 K. The procedure of collecting and evaluating the respective IR data is as follows: (1) In regularily spaced time intervals (4 min) after the admission of the gas mixture of 95 mbar H_2 and 5 mbar O_2 to the MgO sample IR spectra are recorded. (2) For each spectrum the integral absorbance of the hydride bands are determined. (3) These values are then ratioed against the respective integral absorbance obtained after chemisorption of 95 mbar H_2 only.

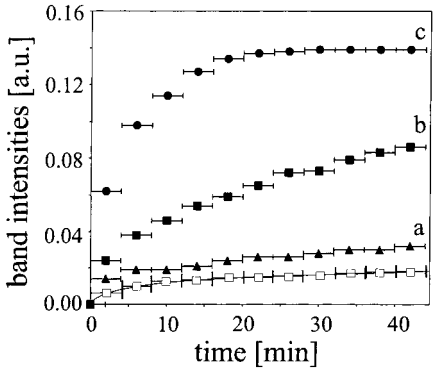

Figure 5. Time dependence of the formation of the isolated OH groups (open symbols: ν(OH) = 3702 cm^{-1}/full symbols: ν(OH) = 3692 cm^{-1}) originating from chemisorption of $H_2/O_2/N_2$ mixtures on MgO at 298 K. The gas compositions were the same as in Figure 2a−c, respectively.

tensities vary uniformly on a time scale of ca. 40 min and additionally depend on the H_2 partial pressure. The respective surface chemical processes should, therefore, somehow be related to the nonsaturation limited complex **II** (eq 2b). On the other hand, for all those spectral features which are unambiguously and exclusively related to the saturation limited complex I (Figures 1 and 2; 3712, 1130, and 3702 cm^{-1}; eq 2a) the influence of $p(H_2)$ is negligibly small.

It has, however, to be emphasized that in both eqs 2a and 2b a hydrogen radical appears as product which has so far remained unaccounted for. It has to be adopted as mobile on the MgO surface and as reactive toward O_2 in the sense of O_2^- formation:

$$H^\bullet + O_2 + O^{2-}-Mg^{2+} \rightarrow O^{2-}(H^+)-Mg^{2+}(O_2^-) \quad (3)$$

As far as the superoxide species are concerned, the surface products according to eqs 2a and b on one hand and to eq 3 on the other, appear to be essentially the same, namely, O_2^-[**A**] and O_2^-[**B**]. The respective EPR signal components clearly show the presence of a neighboring proton via shf coupling (Figure 3). This is in agreement with eqs 2a, 2b, and 3. It disagrees, however, with the following experimental observation: the EPR features attributed to O_2^-[**A**] and O_2^-[**B**] grow with the H_2 partial pressure at the same rate (Figure 3), whereas the IR bands related to the interaction partners OH_{3702} and OH_{3692}, respectively, do not (Figure 2). As mentioned previously the intensity of ν(OH) at 3702 cm^{-1} is saturation limited with respect to $p(H_2)$ and that of ν(OH) at 3692 cm^{-1} strongly depends on $p(H_2)$. A 1:1 assignment of specific OH and O_2^- surface species according to eqs 2a, 2b, and 3 is, therefore, at the present stage, not allowed. In fact, such an assignment would neglect the surface OH groups that give rise to the strong, slightly structured, continuous absorption between 3650 and 3300 cm^{-1}.

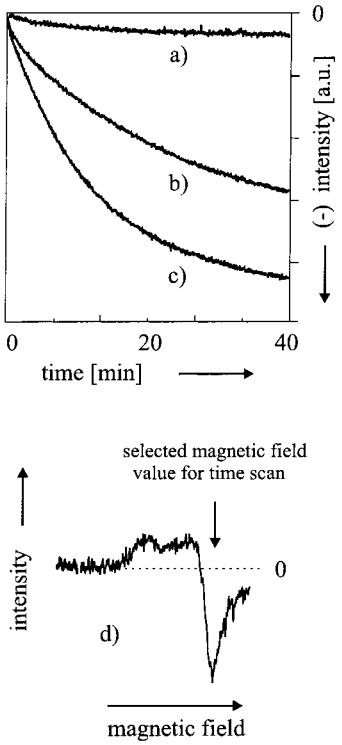

Figure 6. Time dependence of the formation of the O_2^- species originating from chemisorption of $H_2/O_2/N_2$ mixtures at 298 K. The compositions used were the same as those in Figure 2a−c, respectively. The arrow in Figure 6d indicates the magnetic field value at which the intensity measurements were performed.

To quantitate and to compare the rates of intensity changes related to the two surface product species OH^- and O_2^- represented by specific IR and EPR signals, respectively, rate equations have to be established on the empirical basis of the educts involved, namely, surface sites $s^{(i)}$, H_2 and O_2:

$$r_1 = +\frac{d[O_2^-]}{dt} = k_1[s^{(1)}]^{m_1}[H_2]^{n_1}[O_2]^{p_1} \quad (4)$$

$$r_2 = +\frac{d[OH^-]}{dt} = k_2[s^{(2)}]^{m_2}[H_2]^{n_2}[O_2]^{p_2} \quad (5)$$

where t is the time, r_i the reaction rates, k_i the rate constants, and m_i, n_i, and p_i are the reaction orders related to $s^{(i)}$, H_2, and O_2, respectively. These equations do not imply any model of reaction mechanism. The quantities m_i, n_i, and p_i are the reaction orders with respect to the different educt species and must be the same for all products of reaction type i. Of course, the concentrations of the different surface sites $s^{(1)}$ and $s^{(2)}$ are unknown. At an early stage of the reactions ($t \leq 240$ s.) and for not too high H_2 and O_2 pressures they may, however, be considered as constant and are, therefore, included in the rate constants:

$$r_1 = +\frac{d[O_2^-]}{dt} = k_1'[H_2]^{n_1}[O_2]^{p_1} \quad (4a)$$

$$r_2 = + \frac{d[OH^-]}{dt} = k_2'[H_2]^{n_2}[O_2]^{p_2} \qquad (5a)$$

In the first step, the values n_1 and n_2 at constant O_2 partial pressure are determined according to eqs 4a and 5a for those signals that are related to a relevant time dependence of their intensity. These are the IR band at 3692 cm^{-1} (Figures 2 and 5) and the g_{xx} signal component of the EPR spectrum of O_2^-. The comparatively high intensity of the g_{xx} signal component guarantees a reasonable S/N ratio despite intensity consuming experimental conditions: (a) room temperature and (b) the presence of paramagnetic O_2 in the gas phase significantly contribute to signal broadening and, consequently, to loss of sensitivity. The intensity values related to g_{xx} represent the total amount of O_2^- produced on the surface since the contributions of species **A** and **B** are not resolved (Figure 6d). On the other hand the EPR spectra of O_2^- at 77 K (Figure 3) clearly show that the ratio of the abundances of species **A** and **B** is essentially constant in the H_2 pressure interval between 5 and 95 mbar (see the g_{zz} components in Figure 3). Accordingly, in the kinetic evaluation the concentration of O_2^-[**B**] may be replaced by the total concentration of O_2^- which is proportional to the intensity of the g_{xx} component.

In both diagrams, the plots of ln r_1 and ln r_2 against ln [H_2] exhibit straight lines (Figure 7) within the H_2 pressure interval 1 mbar ≤ p(H_2) ≤ 100 mbar. Their slopes are—within the limits of the statistical errors—the same, namely, 0.5 ± 0.1 for n_1 and 0.4 ± 0.1 for n_2. This contributes to the understanding of the reaction mechanism insofar, as it supports a 1:1 assignment of the O_2^-[**B**] species (monitored by EPR spectroscopy) and the OH groups absorbing at 3692 cm^{-1} (monitored by FTIR spectroscopy) in the high H_2 pressure regime (5 mbar < $p(H_2)$ < 95 mbar). Systematic deviations from the model assumptions in terms of (a) varying concentration of reactive surface sites $s^{(i)}$ on MgO and of the gaseous reactants H_2 and O_2 and (b) interference of excessive surface OH and/or O_2^- concentration may be neglected on the basis of the linearity of the plots in Figure 7.

In the second step of the kinetic studies, the reaction order p_2 with respect to O_2 is determined at constant H_2 partial pressures. Only IR data (bands at 3702 and 3692 cm^{-1}), which are easier accessible and more reliable than the detection of O_2^- (see above) were used for the evaluation (Figure 8). Variation of the O_2 partial pressure at $p(H_2)$ = 5mbar gives rise to a monotonic growth of both bands with a larger rate for ν(OH) at 3692 cm^{-1}. As in the case of the reaction order with respect to H_2 (Figure 7) straight lines were obtained in the diagrams ln r_2 against ln [O_2] for both OH bands in question (not shown as figure). The resulting slopes that represent the respective reaction orders p_2 (eq 5a) strongly depend on the H_2 partial pressure as parameters (Figure 9). This is true for both types of OH groups represented by the bands at 3702 and 3692 cm^{-1}. The trends observed (Figure 9) are, at least qualitatively, dictated by the dependence of the relative abundances of the H_2 chemisorption complexes **I** and **II** as educts on the H_2 pressure:[11] below 1 mbar there is nearly exclusively complex **I** (eq 1a) available. Above 1 mbar H_2 complex **II** (eq 1b) is more and more dominating on the surface and p_2 related to the absorption at 3692 cm^{-1} surpasses the value for ν(OH) at 3702 cm^{-1}.

Discussion

Radical O^- centers formed by thermal activation at temperatures above 1078 K under dynamic vacuum conditions may be excluded from the discussion of possible reaction mechanisms at room temperature. EPR spectroscopic measurements under these experimental conditions do not provide any evidence for the presence of O^- species.

In both the coadsorption ($p(H_2)$ < 1 mbar) and the preadsorption experiment (see introduction) predominantly the O_2^-[**A**] species evolves (Figure 3, Table 1). From the bleaching of surface color centers on MgO we already know that this radical type can be formed at a single well-defined surface element,

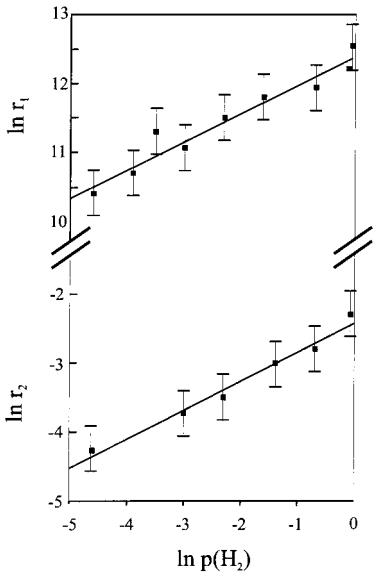

Figure 7. Double logarithmic plot of the reaction rate related to the formation of (a) O_2^-[B] and (b) OH_{3692} versus H_2 concentration. The errors indicated in Figure 7 are based on statistical fluctuations of the determination of the respective integrated signal intensities (EPR and IR, respectively) and their propagation into the values of the logarithmic reaction rate (ln r_1 or ln r_2)

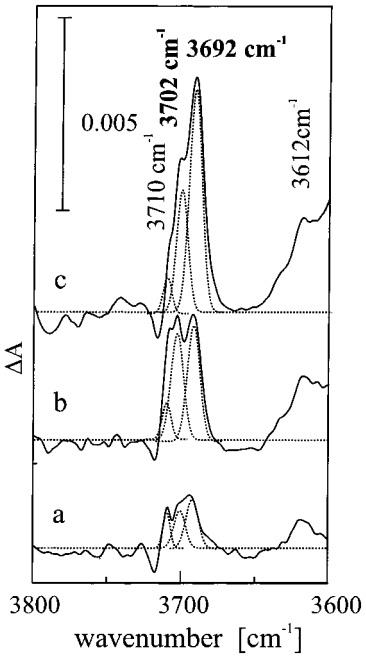

Figure 8. IR difference spectra recorded in the OH stretching region of MgO after surface reaction with $H_2/O_2/N_2$ mixtures at 298 K (time scale: 12−16 min after gas admission). Gas composition: (a) 5:5:90 mbar, (b) 5:50:45 mbar, and (c) 5:95:0 mbar (the H_2 partial pressure is constant!). Each curve was obtained by subtracting the absorbance spectrum related to chemisorption of pure H_2 from that related to chemisorption of H_2 plus O_2.

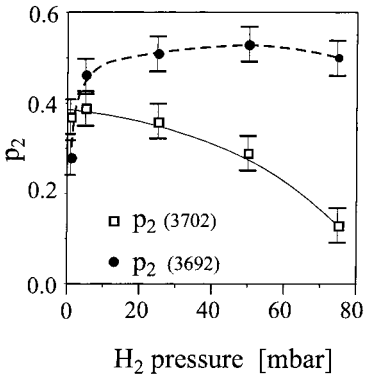

Figure 9. Plot of the reaction orders p_2 related to the OH stretching bands at 3702 and 3692 cm^{-1}, (see eqs 5a and 5b) with respect to O_2 against the H_2 partial pressure. The errors indicated in Figure 9 are based on statistical fluctuations of the determination of the respective integrated signal intensities and their propagation into the values of p_2.

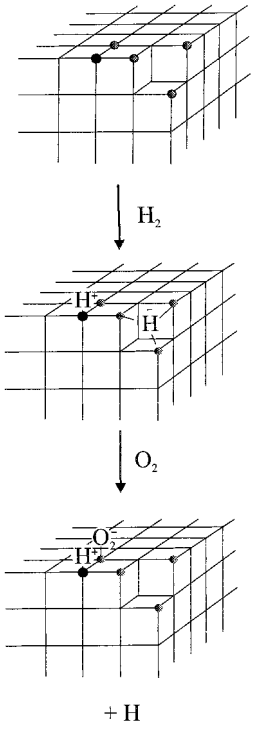

Figure 10. Model of the local MgO surface structure involved in the formation of chemisorption complex **I** (eq 1a) and its oxidation by molecular oxygen (eq 2a) according to ref 16.

namely, a low-coordinated ion pair, the cation of which is a constituent of an anion vacancy (Figure 10).[4,11,16]

Because of the limited mobility of charged species on the ionic surface, the H_2 chemisorption (irreversible type I, eq 1a) and the formation of the complex O_2^- [**A**] after the electron transfer must occur within the same local surface element. This suggests that the Mg^{2+} hosting the hydride should also be the complexing cation for O_2^-. As this cation is low coordinated it should evoke a relatively high crystal field splitting. In fact, this is in conflict with the EPR observation of O_2^-[**A**]. Previous studies[16−19,22,31] and theoretical calculations[32] led to the conclusion that the complexing cation must be 5-fold coordinated which means that it lies in a (100) microplane. The question arises why the O_2^- is not complexed by the electrostatically more favorable low coordinated cation (see above).[16] The answer is likely to be related to the electronic interaction between the O_2^- species and the OH group. It stabilizes the O_2^-[**A**] species

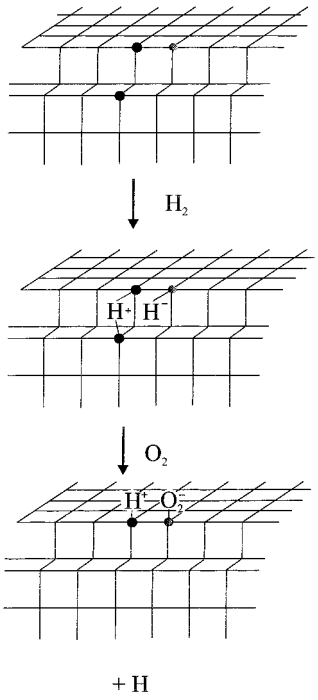

Figure 11. Model of the local MgO surface structure involved in the formation of chemisorption complex **II** (eq 1b) and its oxidation by molecular oxygen (eq 2b).

in the $Mg^{2+}{}_{5C}\cdots O_2^-$ complex such that its abundance dominates all other possible complexes based on lower coordinated Mg^{2+} cations.[30] In our experiments (at 77 K) O_2^-[**A**] species without shf have never been observed. According to ref 16 and in agreement with these considerations the structure model of Figure 10 was developed.

In the coadsorption experiment the rise of the H_2 pressure significantly increases the surface concentration of both O_2^-[**A**] and O_2^-[**B**] (Figure 3) as well as of the OH groups absorbing at 3692 cm^{-1} (Figure 2). This is due to the increasing abundance of the reversible complex **II**. Its oxidation with O_2 directly implies OH groups interacting with O_2^- at the site of complex **II** (eq 2b). This would already explain the time and $p(H_2)$ correlated signals of O_2^- [**B**] and of ν(OH) at 3692 cm^{-1}. The appearance of O_2^-[**A**] is intimately related to the additional production of neutral H atoms according to eq 2b. They form $OH\cdots O_2^-$ surface complexes (both types), provided $H^\bullet$ and O_2 meet on the surface at an appropriate $O^{2-}-Mg^{2+}$ ion pair. These may, but need not necessarily be the sites where complex **I** and **II** are located (Figures 10 and 11). The interesting point is that the interaction between OH_{3692} and O_2^-[**B**] appears to be independent of the origin of the OH group: complex **II** (eq 2b) or $H^\bullet$ radical reduction (eq 3).

As mentioned previously, the OH group of the reversibly formed complex **II** is strongly influenced by an appropriately spaced and sufficiently strong proton acceptor (eq 1b). Neighboring O^{2-} ions on (110) microplanes, in other words on monatomic steps, would provide an $O^{2-}\cdots O^{2-}$ distance of about 2.96 Å which is the most suitable one for strong H bond interactions (Figure 11).[25] This statement appears to be in conflict with the weak H bond formed after the oxidation of the hydride group with O_2: The resulting surface complex $OH_{3692}\cdots O_2^-$[**B**] reveals an H-bond induced shift with respect to free and isolated OH groups (~3712 cm^{-1}) of 20 cm^{-1} only. It should, however, be kept in mind that the hydride oxidation creates OH groups in addition to those originating from chemisorption—OH groups which stem from the surface mobile

$H^{\bullet}$ radical of eq 3. Thus the O^{2-} previously involved as proton acceptor in the chemisorption complex **II** (eq 2b) may well be subject to a chemical change induced by an $H^{\bullet}$ radical. The continuous absorption in the OH stretching region indicates that so far unspecifiable OH groups emerge on the MgO surface in the course of the hydride oxidation. Therefore, the $OH_{3692}\cdots O_2^-$[**B**] interaction may not be considered isolated from the environment.

Another phenomenon which has so far remained uninterpreted, also appears to be related to the continuous absorption: H bonds between neighboring surface OH groups are likely in the surface model presented here and would give rise to unspecific broad absorptions rather than to specific signals such as $\nu(OH_{3702})$. This may—even though on a speculative basis—explain the different influence of $p(H_2)$ on the intensity of the relevant spectroscopic signals of the interaction partners in the complex $OH_{3702}\cdots O_2^-$[**A**] (Figures 2 and 3). $\nu(OH_{3702})$ is saturation limited and the signal components related to O_2^-[**A**] are not. The coordination state of the cation of O_2^-[**B**] is significantly lower than that of O_2^-[**A**][16,17,21,22,30], in agreement with the above-mentioned surface structure of complex **II** (compare Figures 11 with 10). The reaction product O_2^-[**B**] is likely to be complexed by the 4-coordinated cation hosting previously the hydride group.[21]

In essence, the local surface structures to which the two types of superoxide anion species may be attached, are the ion pairs $O^{2-}{}_{4C}$ and $Mg^{2+}{}_{5C}$ (Figure 10) and $O^{2-}{}_{4C}$ and $Mg^{2+}{}_{4C}$ (Figure 11). Obviously the presence of a 3-coordinated anion vacancy (removed corner anion)[16] or a monatomic step in the structure models of Figures 10 and 11, respectively, is not a prerequisite for the $H^{\bullet}$ radical induced redox step (eq 3). It is, however, a necessary requirement for heterolytic H_2 splitting (eqs 1a and 1b), followed by the initial redox reactions (eqs 2a and 2b).

The evaluation of the kinetic data related to O_2^-[**B**] (eq 4) and OH_{3692} (eq 5) as products (Figure 7) provides equal and constant broken reaction orders with respect to H_2 in the pressure interval between 5 and 100 mbar. This reveals that the constituents of the product pair O_2^-[**B**]$\cdots OH_{3692}$ have a common reactive history and that the overall reaction mechanism does—irrespective of its complicacy—not change in the indicated interval of H_2 partial pressure. The O_2^- related to the charge transfer from either H^- (hydride) or $H^{\bullet}$ (radical) to O_2 (eqs 2b and 3, respectively) always meets an OH group—either out of the chemisorption or out of the redox process based on the $H^{\bullet}$ radical—in the close vicinity.

Conclusion

The products of coadsorption of H_2 and O_2 on the surface of MgO nanoparticles are pairs of O_2^- and OH interacting via specific intermolecular forces. There are two different types of these pairs. The oxygen ions of the OH groups are uniformly 4-coordinated and thus located on crystallite edges, whereas the complexing cation for the O_2^- species is either 5- or 4-coordinated (O_2^-[**A**] or O_2^-[**B**], respectively). The electronic H-bond-like interaction between O_2^- and OH probably contributes to the stability of the $Mg^{2+}...O_2^-$ complexes even at room temperature.[30] Not all of the described ion pairs hosting the reaction products (O_2^-, OH) are located there where heterolytic H_2 splitting occurs, namely next to a 3-coordinated anion vacancy[16] (Figure 10, eq 2a) or within a (110) microplane (Figure 11, eq 2b). This is due to the reaction of the surface mobile $H^{\bullet}$ radical with O_2 (eq 3) which obviously leads to the same reaction products (O_2^-, OH, same coordination states for the involved ion pair), but does not underlie the additional surface structural constraints of heterolytic H_2 splitting (eqs 1a and 1b; Figures 10 and 11). Remains the requirement that the O^{2-} anion involved is located in any arbitrary type of edge including those defining double vacancies on the surface.[33−35]

There is plenty of kinetic data related to the oxidative coupling reaction of methane (OCM[36−39]) which indicate that low coordinated ion pairs on MgO or other metal oxides play a crucial role in the activation of methane.[39] Conclusive evidence has, however, so far not been provided whether heterolytic bond splitting is in fact the decisive initial step in the OCM process,[34] as it is in the H_2/O_2 coadsorption experiment at room temperature. Therefore, CH_4/O_2 coadsorption studies following the strategic guidelines presented here may considerably facilitate the search for the reaction mechanism of the OCM process as well as the endeavor of improving the respective catalysts. The complementary character of the IR and EPR data would be the highlight of this type of research as it was in the present one. It should, however, be emphasized that the reliability of this synopsis and the inherently derived surface model may be further improved by subjecting the MgO sample in the relevant IR and EPR experiments to the same temperature (77 K).

Acknowledgements. Considerable financial support from the Fonds zur Förderung der Wissenschaftlichen Forschung (FWF Contract No. P11542-CHE and P14731-CHE) and the Max-Bruckner-Stiftung (MBFST Contract No. 2149) is gratefully acknowledged.

References and Notes

(1) Coluccia, S.; Tench, A. J. In *Proceedings of the 7th International Congress on Catalysis B*; Seyama, T., Tanabe, K., Eds.; Kodansha: Tokyo, 1981; p 1154.

(2) Martra, G.; Cacciatori, T.; Marchese, L.; Hargreaves, J. S. J.; Mellor, I. M.; Joyner, R. W.; Coluccia, S. *Catal. Today* **2001**. In press.

(3) Anpo, M.; Yamada, Y.; Kubokawa, Y.; Coluccia, S.; Zecchina, A.; Che, M. *J. Chem. Soc., Faraday Trans. 1* **1988**, *84*, 751.

(4) Murphy, D. M.; Farley, R. D.; Purnell, I. J.; Rowlands, C. C.; Yacob, A. R.; Paganini, M. C.; Giamello, E. *J. Phys. Chem. B* **1999**, *103*, 1944.

(5) Giamello, E.; Paganini, M. C.; Murphy, D. M.; Ferrari, A. M.; Pacchioni, G. *J. Phys. Chem. B* **1997**, *101*, 971.

(6) Pinarello, G.; Pisani, C.; D'Ercole, A.; Chiesa, M.; Paganini, M. C.; Giamello, E.; Diwald, O. *Surf. Sci.* **2001**. In press

(7) Henrich, V. E.; Cox, P. A. *The Surface Science of Metal Oxides*; Cambridge University Press: Cambridge, 1994.

(8) Che, M., Bond, C., Eds. *Adsorption and Catalysis on Oxide Surfaces*; Elsevier: Amsterdam, 1985.

(9) Lambert, R. M., Pacchioni, G., Eds. *Chemisorption and Reactivity on Supported Clusters and Thin Films*; Nato ASI Series 331; Kluwer Academic Publishers: Dordrecht, 1997.

(10) Coluccia, S.; Boccuzzi, F.; Ghiotti, G.; Morterra, C. *J. Chem. Soc., Faraday Trans. 1* **1982**, *78*, 2111.

(11) Diwald, O.; Hofmann, P.; Knözinger, E. *Phys. Chem. Chem. Phys* **1999**, *1*, 713.

(12) Ito, T.; Sekino, T.; Moriai, N.; Tokuda, T. *J. Chem. Soc., Faraday Trans. 1* **1981**, *77*, 2181.

(13) Cordischi, D.; Indovina, V.; Occhiuzzi, M. *J. Chem. Soc., Faraday Trans. 1* **1978**, *74*, 456.

(14) Ito, T.; Yoshioka, M.; Tokuda, T. *J. Chem. Soc., Faraday Trans. 1* **1983**, *79*, 2277.

(15) Knözinger, E.; Sterrer, M.; Diwald, O. *J. Mol. Catal. A: Chem.* **2000**, *162*, 83.

(16) Giamello, E.; Paganini, M. C.; Chiesa, M.; Coluccia, S.; Martra, G.; Murphy, D. M.; Pacchioni, G. *Surf. Sci.***1999**, *421*, 246.

(17) Che, M.; Tench, A. J. *Adv. Catal.* **1983**, *32*, 1.

(18) Anpo, M.; Che, M.; Fubini, B.; Garrone, E.; Giamello, E.; Paganini, M. C. *Top. Catal.* **1999**, *8*, 189.

(19) Kanzig, W.; Cohen, M. H. *Phys. Rev. Lett.* **1959**, *3*, 509.

(20) Diwald, O.; Knözinger, E.; Martra, G. *J. Chem. Phys.* **1999**, *111*, 6668.

(21) Giamello, E.; Garrone, E.; Ugliengo, P.; Che, M.; Tench, A. J. *J. Chem. Soc., Faraday Trans. 1* **1989**, *85*, 3987.

(22) Giamello, E.; Ugliengo, P.; Garrone, E. *J. Chem. Soc., Faraday Trans. I* **1989**, *85*, 1373.

(23) Garrone, E.; Giamello, E.; Ferraris, M.; Spoto, G. *J. Chem. Soc., Faraday Trans. I* **1992**, *88*, 333.

(24) Knözinger, E.; Jacob, K.-H.; Singh, S.; Hofmann, P. *Surf. Sci.* **1993**, *290*, 388.

(25) Knözinger, E.; Jacob, K. H.; Hofmann, P. *J. Chem. Soc. Faraday Trans. I* **1993**, *89*, 1101.

(26) Furthermore a third O_2^- species, called **B′**, appears to a lesser extent. The principal values for the **g** matrix are essentially the same as those of the O_2^- species **B**. They do, however, not exhibit any shf splitting at 77 K.

(27) Shiotani, M.; Moro, G.; Freed, J. H. *J. Chem. Phys.* **1981**, *74*, 2616.

(28) Chamulitrat, W.; Kevan, L. *J. Phys. Chem.* **1985**, *89*, 4989.

(29) Dyrek, K.; Adamski, A.; Sojka, Z. *Spectrochim. Acta A* **1998**, *54*, 2337.

(30) Diwald, O.; Sterrer, M.; Knözinger, E. To be published.

(31) Giamello, E.; Murphy, D.; Garrone, E,; Zecchina, A. *Spectrochim. Acta A* **1993**, *49*, 1323.

(32) Pacchioni, G.; Ferrari, A.; Giamello, E. *Chem. Phys. Lett.* **1996**, *56*, 255.

(33) Lunsford, J. H.; Jayne, J. P. *J. Phys. Chem.* **1966**, *70*, 3463.

(34) Ojamäe, L.; Pisani, C. *J. Chem. Phys*. **1998**, *109*, 10984.

(35) Sterrer, M.; Diwald, O.; Knözinger, E. *J. Phys. Chem. B* **2000**, *104*, 3601.

(36) Lunsford, J. H. In *Handbook of Heterogeneous Catalysis*; Ertl, G., H. Knözinger, H., Weitkampp, J., Eds. VCH: Weinheim **1997**; Vol. 4, p 843.

(37) Dissanayke, D.; Lunsford, J. H.; Rosynek, M. P. *J. Catal.* **1993**, *143*, 286.

(38) Sokolovskii, V. D.; Aliev, S. M.; Buyevskaya, O. V.; Davydov, A. A. *Catal. Today* **1989**, *4*, 293.

(39) Ito, T.; Tashiro, T.; Kawasaki, M.; Watanabe, T.; Toi, K.; Kobayashi, H. *J. Phys. Chem.* **1983**, *95*, 4476.